Int. J. Electrochem. Sci., 7 **(2012)** 8337 - 8355

International Journal of
ELECTROCHEMICAL
SCIENCE
www.electrochemsci.org

The Deposition Process and the Properties of Direct Electroless Nickel-Phosphorous Coating with Chromium-Free Phosphate Pickling Pretreatment on AZ31 Magnesium Alloy

Haiping Liu, Sifu Bi, Lixin Cao, Qingyou Bai, Xiangguo Teng, Yuanchun Yu*

School of Marine Science and Technology, Harbin Institute of Technology, Weihai 264209, China;
*E-mail: bisifu@126.com

Received: 17 July 2012 / *Accepted:* 12 August 2012 / *Published:* 1 September 2012

A direct electroless nickel-phosphorous (Ni-P) coating was obtained on AZ31 magnesium alloy after dipping in phosphate pickling bath. The deposition process and the properties of Ni-P coating on magnesium alloy were investigated by measuring open potential-time curves in situ and polarization curves in combination with X-ray fluorescene spectrometry, X-ray diffractometer and scanning electron microscopy. The results showed that after phosphate pickling pretreatment, the Mg-Mn phosphate film formed on magnesium alloy surface made the electrode potential of magnesium alloys shift to the positive direction. The Ni-P coating was compact, uniformly covered the magnesium alloy surface, with high phosphorus content (for about 10.3 wt%). The hardness of electroless Ni-P coating for 60 min was 552.4 HV, which is far higher than that of the Mg alloy substrate. The corrosion potential of electroless Ni-P coating for 60 min was -0.323 V *vs.* SCE, and shifted to the positive direction by 1198 mV, as compared to magnesium alloy substrate. The corrosion resistance of the magnesium alloy could be greatly increased by the formations of Mg-Mn phosphate film and electroless Ni-P coating.

Keywords: Magnesium alloy; phosphate pickling; electroless plating; Ni-P coating; corrosion resistance

1. INTRODUCTION

Magnesium alloys attract great attention in aerospace, automobile and electronic industries since they have low density, high specific strength and good mechanical and damping characteristics[1, 2]. However, being a highly active metal alloy, magnesium alloys have poor atmospheric corrosion resistance and wear resistance, which restricts their extensive utilization. Therefore, a wide variety of surface treatments, such as anodic oxidization[3, 4], micro-arc oxidization[5], electro/electroless plating[6-8], plasma electrolytic oxidation (PEO)[9], and protective diffusion coatings[10, 11] are introduced to enhance these properties of magnesium alloys. Among them, electroless nickel-phosphorus (Ni-P) coating is of special interest, due to its uniform deposition, good corrosion and wear resistance, good electrical, and good solderability[12-14].

However, the Ni-P / Mg system is a classical example of cathodic coating on an anodic substrate and the adhesion of Ni-P coating on magnesium substrate is very poor. Thus, the protective ability of electroless Ni-P coating on magnesium alloy is limited by porosity in Ni-P coating and the poor adhesion. Hence, a number of pretreatment processes such as zinc immersion and conversion treatments were applied to magnesium alloy prior to electroless nickel plating [15, 16]. The role of the pretreatment process is the formation of an intermediate layer on the substrate, which could reduce the potential difference between the substrate and the Ni-P coating and reduce the corrosion of the magnesium alloy during electroless nickel process. According to the previous reports, the pretreatment solutions often contained hexavalent chromium and cyanide [17, 18], which are restricted due to their high toxicity to the environment. Recently, the chromium-free environmental and health friendly technologies such as molybdate, phosphate and phytic acid have been studied to inhibit the magnesium alloy corrosion[18-23].

Generally, an alkaline or near-neutral electroless nickel bath is preferred for magnesium and its alloys since magnesium alloys are easily corroded in the acidic nickel bath[24]. There are many researches in the electroless nickel coating properties on magnesium alloy. Zhenmin Liu *et al* [2] studied the effect of the magnesium alloy substrate microstructure and roughness on the deposition rate, nucleation, coating microstructure, and mechanical property of Ni-P coatings. Y.W. Song *et al* [6] and Shiyan Zhang *et al* [25] improved the corrosion resistance of AZ91D magnesium alloy by depositing Ni-P-ZrO_2 or Ni-P-TiO_2 composite coatings and multilayer coatings on magnesium alloy substrates. Yanping Zhu *et al* [15] investigated the interface reactions and film features of AZ91D magnesium alloy in pickling, activation and zinc immersion solutions. Rajan Ambat *et al* [17] studied the effect of substrate microstructure and plating parameters on electroless nickel-plating on AZ91D magnesium alloy, obtained Ni-P coating with 7 wt.% P and a hardness value of 600-700 VHN. Jianzhong Li *et al* [26, 27] investigated the effect of the plating solution on the properties and structures in using $NiSO_4 \cdot 6H_2O$ as the main salt in alkaline electroless nickel solutions. However, not much information is available regarding the direct electroless nickel plating process and the properties of Ni-P coating with an environmental friendly pretreatment process of magnesium alloy.

In our previous experiments, an environmental-friendly phosphate pickling pretreatment films was obtained on the magnesium alloy[28]. After that, electroless Ni-P coating from a near-neutral bath using sulfate nickel as the main salt was obtained on the pretreated magnesium alloys[29]. This phosphate pickling bath and the electroless nickel bath are also used in the present study. Open circuit potential during the immersion or electroless plating deposition process reflects the variation of the electrode surface state, which is extensively used to evaluate different deposition processes[15, 30].

Being a highly active metal, electroless plating of magnesium alloy needs special bath formulations and pre-cleaning treatments. Hence, the direct electroless Ni-P plating of magnesium is still a challenge and the process is still more complicated for the researchers. Therefore, in this paper, the phosphate pickling pretreatment and the deposition process on AZ31 magnesium alloy are investigated by in situ measurement of the open potential-time curves. In addition, the properties such as micro-structure, hardness and corrosion characteristics of the magnesium alloy after direct electroless Ni-P plating are also studied.

2. EXPERIMENTAL

AZ31 magnesium alloys samples with dimension of 30 mm×30 mm×3 mm, were used as electroless nickel plating substrate. All the samples were ground with 1000 grade SiC sandpaper before electroless Ni-P plating so as to obtain uniform surfaces. After sanding, the substrates were cleaned in an alkaline bath to remove soils or greases on magnesium alloy surface and rinsed thoroughly in deionized water to remove all the alkali. Then the magnesium alloy samples were immersed in the phosphate pickling bath for 5 min at 20 °C, where 30 ml/L H_3PO_4(85% V/V) and 5 g/L $Mn(H_2PO_4)_2$, 50 ml/L HNO_3(80%V/V), 150 ml/L acetic acid were the main ingredients. After being rinsed in deionized water, the samples were immersed in the electroless nickel solution for plating Ni-P coating at 80 °C, where 18 g/L $NiSO_4 \cdot 6H_2O$, 24 g/L $NaH_2PO_2 \cdot H_2O$, 5 g/L citric acid, 13 g/L sodium acetate, 8 g/L NH_4HF_2, 12 ml/L HF (40%V/V), 2 mg/L thiourea were contained with pH 6.4. The chemicals used in this research were all of analytical grade. Following these pretreatments, an electroless Ni-P coating is deposited on magnesium alloy.

The surface morphology of different samples was examined by scanning electron microscopy (SEM) (TESCAN VEGAII). X-ray fluorescence spectrometer (XRF) (BrukeraxsS4 Explorer, Germany) was made to confirm the coating thickness and composition of magnesium alloys after phosphate pickling pretreatment and electroless Ni-P plating. The crystalline structures of the samples were analyzed using X-ray diffractometer (XRD, DX2700, Dandong) with a Cu target and a monochromator at 40 kV and 30 mA with the scanning rate 0.02 °/s. The hardness of the magnesium alloy and the Ni-P coatings were evaluated using a HXD-1000TB micro-hardness machine, at a load of 50 g and a duration time of 15 s.

In this paper, the open potential during pickling pretreatment process or electroless Ni-P process on magnesium alloy was recorded as a function of time in a three-compartment Pyrex cell using a CHI electrochemical station (model 660A). The magnesium alloy substrates were first sealed using insulated adhesive tape, except for a 1 cm×1 cm effective working area, then pretreated by alkaline cleaning. After thoroughly rinsing in deionized water, the samples were immediately dipped in phosphate pickling bath or electroless nickel solutions as working electrodes for the open potential-time curves measurements.

The corrosion resistance of samples was measured by polarization curves test in a CHI electrochemical station (model 660A). The polarization curves experiments were performed in a 3.5 wt.% NaCl solution open to air and at room temperature. A three compartment Pyrex cell with the different films on magnesium alloys as the working electrode, platinum plate as the counter electrode, and a saturated calomel electrode (SCE) as the reference electrode was used in the tests. All potentials were determined with respect to this reference electrode and were controlled by a conventional potentiostat with a programmer.

3. RESULTS AND DISCUSSION

3.1 Phosphate pickling pretreatment process on AZ31 magnesium alloy

The surface morphology and the corresponding energy dispersive spectrometer (EDS) spectrum of AZ31 magnesium alloy after sanding are presented in Figure 1. According to Figure 1, magnesium alloy mainly contains Mg, O, and Al elements with obvious polished stripes on the surface.

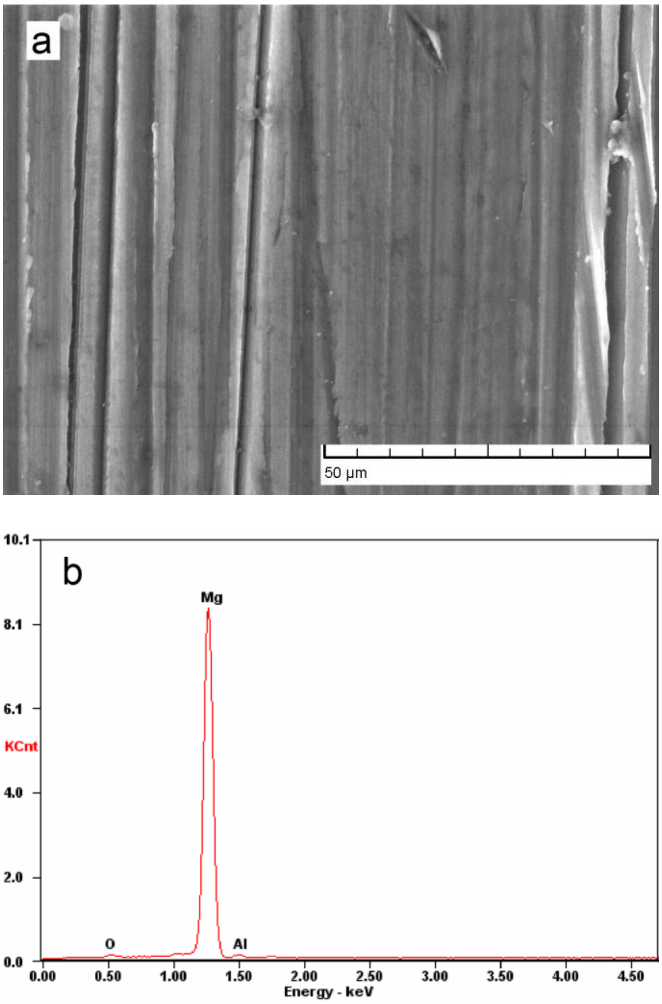

Figure 1. SEM micrograph (a) and the corresponding EDS spectrum (b) of AZ31 magnesium alloy after sanding

Figure 2 show the surface morphology of magnesium alloy after phosphate pickling pretreatment. The optical image in Figure 2(a) displays that an inhomogeneous film was obtained on the magnesium alloy surface. Moreover, it can be seen from Figure 2(b) and 2(c) that this film is discontinuous with some deep and wide cracks on the magnesium alloy surface.

Since the phosphate pickling film is inhomogeneous, the film compositions of different regions marked in figure 2(c) are detected by EDS analysis shown in Figure 3 and Table 1. According to

Figure 3 and Table 1, the element composition in area I (the dark region) is similar to that of magnesium alloy substrate for they mainly contain Mg, O, and Al elements.

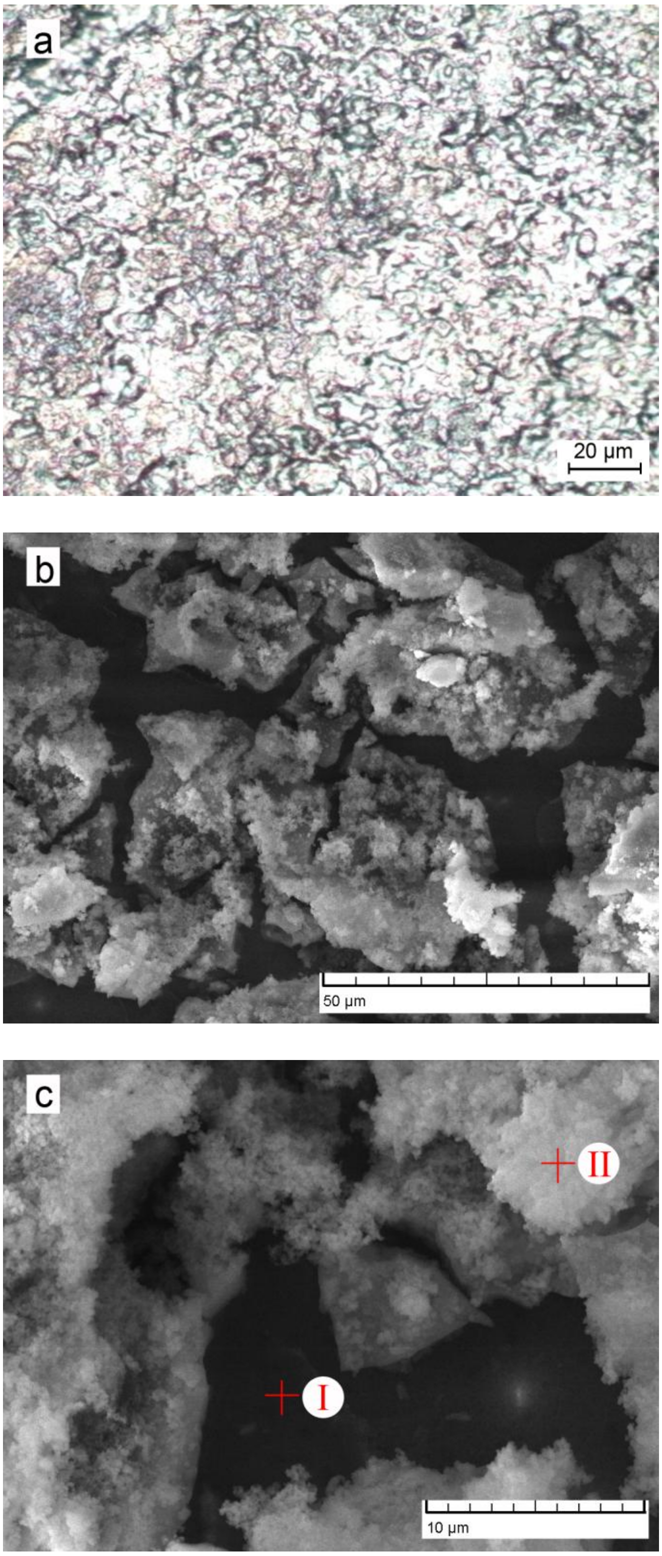

Figure 2. the Optical image and SEM micrographs of magnesium alloys after phosphate pickling pretreatment, (a) optical image; (b) SEM image; (c) a higher magnification of Figure 2(b)

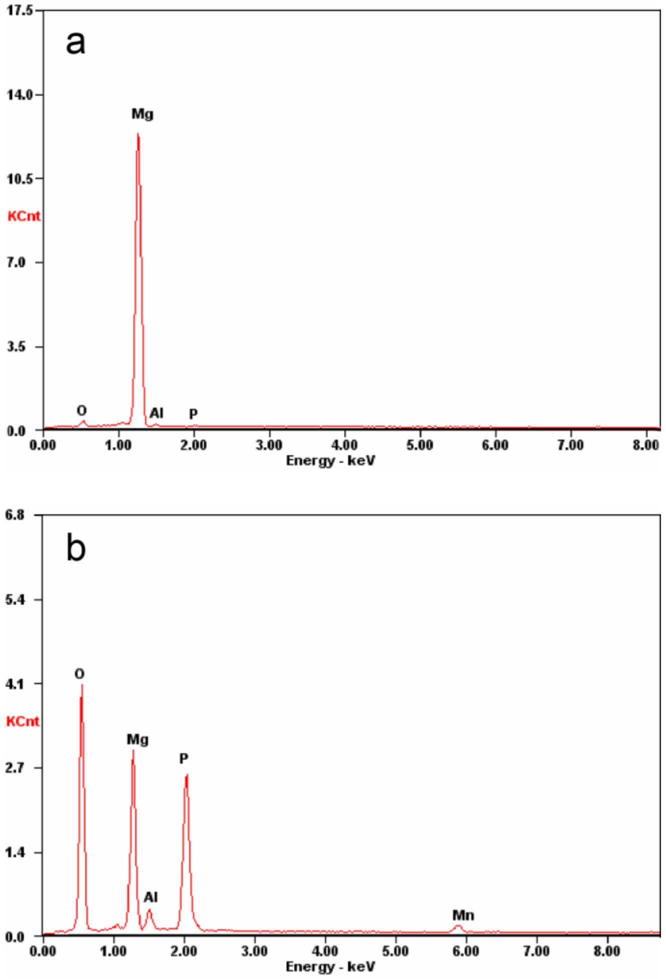

Figure 3. the Corresponding EDS spectra of magnesium alloy after phosphate pickling pretreatment from Figure 2(c): (a) dark region (area I); (b) white region (area II)

Table 1. Chemical compositions of magnesium alloy before and after phosphate pickling pretreatment (in wt%) obtained by EDS analyses

Element	Before	area I after pretreatment	area II after pretreatment
O	2.59	5.78	55.22
Mg	94.88	90.59	20.21
Al	2.53	2.55	2.73
P	0.00	1.08	19.24
Mn	0.00	0.00	2.60

However, after phosphate pickling, the content of Mg is decreased greatly while P and Mn elements are detected in the area II (white region). Compared with the composition of Mg alloy substrate, it can be deduced that the Mg and Al may come from magnesium alloy substrate while P and Mn come from phosphate pickling process. The higher concentration of O element in the area II (for about 55.22%), may come from both the substrate and the phosphate pickling process. Therefore, it can be concluded that a discontinuous film contained Mg, Mn, O and P elements was formed on the magnesium alloy after phosphate pickling pretreatment.

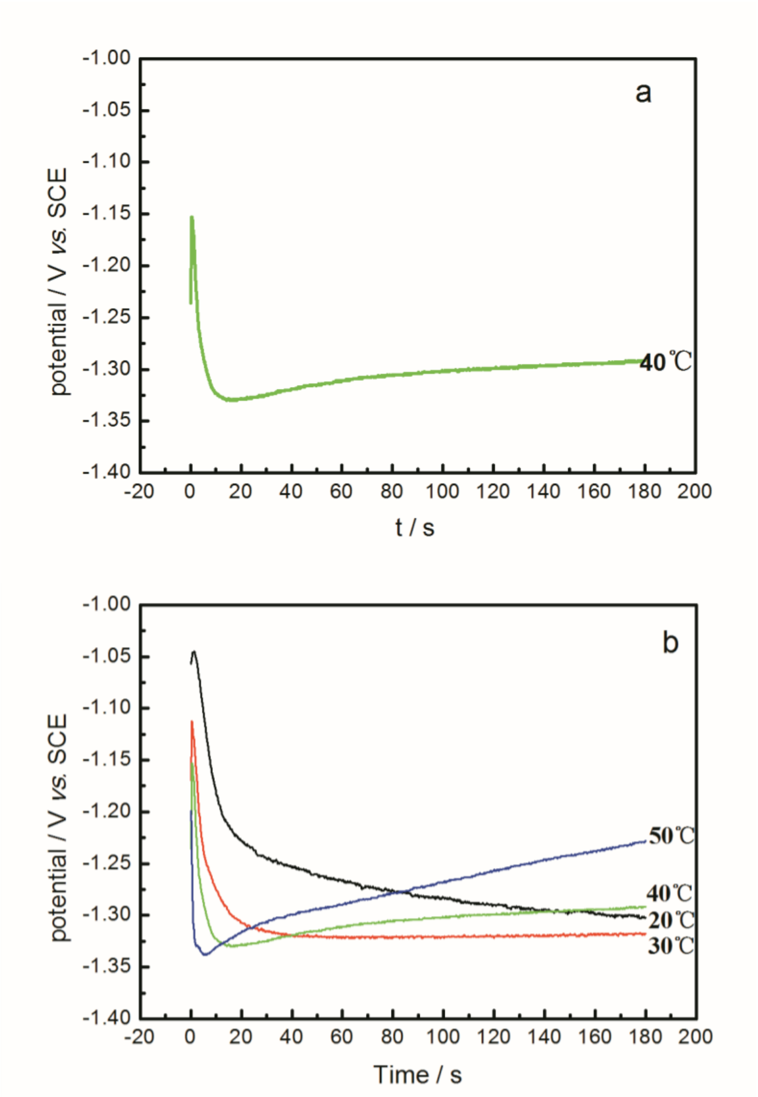

Figure 4. open potential-time curves of phosphate pretreatment on magnesium alloy substrate at different temperature.

In order to gain more insight about the growth process of the film formation, we studied the open potential-time curve during the phosphate pickling pretreatment process at different temperature (Figure 4). According to Figure 4(a), as dipping magnesium alloy electrode into phosphate pickling solution, the open potential first shows a negative shifting and then a positive shifting. Moreover, Figure 4(b) indicates that the duration time of the negative shift on electrode potential is related to the solution temperature. Thus, a higher temperature leads to a shorter negative shifting time. For example, at 20 °C open circuit potential has been in the negative direction within 180 s; while at 50 °C, the negative shift time is no more than 10 s.

From the experimental results, it is clear that the changes in open potential during the phosphate pickling pretreatment process could reflect the variation of the magnesium surface state. In this paper, the phosphate pickling bath mainly contains H_3PO_4 and $Mn(H_2PO_4)_2$. When magnesium alloy is immersed in the pickling bath, the oxides and hydroxides on the Mg substrate surface are quickly dissolved away due to reaction with H^+ in the bath. The initial negative shifting of the potential could be related to the dissolved reaction of MgO and $Mg(OH)_2$ and the hydrogen evolution reaction.

The magnesium alloy has an inhomogenous microstructure for consisting of α phase (Mg, mainly phase) and β phase ($Mg_{17}Al_{12}$, second phase)[6, 16]. These two phases have different electrochemical activity due to their different electrode potential [15, 18], which can result in many micro-corrosion cells on the surface when magnesium alloy was immersed in the phosphate pickling solutions. Thus, at the micro-anode zone (α phase with lower potential), magnesium is dissolved, while at the micro-cathode (β phase with higher potential), H^+ accepts the electrons from the micro-anode zones and is reduced.

$$Mg - 2e^- \rightarrow Mg^{2+} \qquad (1)$$

$$2H^+ + 2e- \rightarrow H_2\uparrow \qquad (2)$$

Moreover, as dipping the magnesium alloy into the phosphate pickling bath, a number of different simultaneous electrochemical reactions also occur at the interface between magnesium and the solution. These processes are as follows:

$$H_2PO_4^- \rightarrow PO_4^{3-} + 2H^+ \qquad (3)$$

$$2PO_4^{3-} + 3Mg^{2+} \rightarrow Mg_3(PO_4)_2 \qquad (4)$$

$$2PO_4^{3-} + 3Mn^{2+} \rightarrow Mn_3(PO_4)_2 \qquad (5)$$

Insoluble $Mg_3(PO_4)_2$ and $Mn_3(PO_4)_2$ were then formed on the magnesium alloy surface. The presence of discontinuous film consisted of Mg, Mn, O and P elements on magnesium alloy after pretreatment might support this argument (Figure 2 and Figure 3). So it can be concluded that the film after phosphate pickling pretreatment is composed of much $Mg_3(PO_4)_2$ and a small quantity of $Mn_3(PO_4)_2$. Moreover, the discontinuous film on Mg alloy substrate may be related to the different surface activity of magnesium alloy. On the other hand, the formation of H_2 gas during the phosphate pickling process may also cause film surface cracks.

It's the formation of Mg-Mn phosphate film caused the magnesium electrode potential to shift to the positive direction, and a shorter negative shifting time at higher temperature means a faster film growth rate. When the film formed, the open circuit potential stabilized at around -1.3- -1.2 V (*vs* SCE), while the standard electrode potential of magnesium is -2.4 V. The positive shifting of the electrode potential after the formation of the film will reduce the potential difference between the substrate and Ni-P coating, and will help improve the corrosion resistance of magnesium during electroless Ni-P deposition process.

It should be noted that from Figure 4(b), the open circuit potential always shifted in a negative direction at 20 °C, which means that the temperature may be too low for the film formation. At 30 °C, this positive shift of the potential is not clear; while at 40 °C and 50 °C, the positive shift is very obvious, indicating that a higher temperature is conducive to film formation. However, the too high temperature usually accelerates the corrosion of magnesium alloy substrate. In addition, a thick film will reduce the adhesion strength of the coating to the substrate. Therefore, in order to obtain an excellent film, the right temperature and film thickness should be chosen.

3.2 Electroless Ni-P process

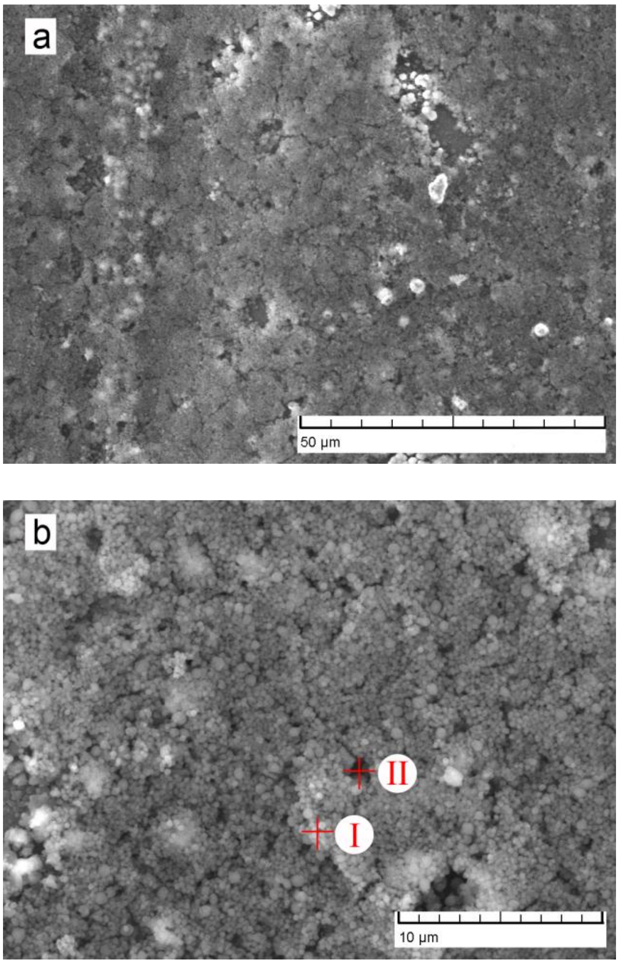

Figure 5. SEM micrographs, (a) electroless Ni-P coating on magnesium alloy deposited for 1 min; (b) a higher magnification of Figure 5(a)

A discontinuous $Mg_3(PO_4)_2$ and $Mn_3(PO_4)_2$ film as former shows was covered on AZ31 magnesium alloy surface after phosphate pickling pretreatment. After that, the electroless Ni-P coating was directly deposited on this basis. Figure 5 shows the SEM morphology of electroless Ni-P coating on magnesium alloy deposited for 1 min. According to Figure 5(a), after electroless Ni-P for 1 min, the magnesium alloy exhibits a smooth and compact surface, which is very different with that after phosphate pickling pretreatment. However, in this Ni-P coating, a nonuniform distribution of the components is observed from the clear white and dark areas. SEM micrograph at higher magnification (Figure 5(b)) shows that, spherical Ni-P crystal filled the gaps at the surface and does not cover the whole substrate.

To investigate the composition of white and dark region marked as I and II in Figure 5 (b), we studied the Ni-P coatings by EDS analysis, as shown in Figure 6 and Table 2. According to EDS results, this Ni-P coating deposited for 1 min mainly contains Mg, F, Na, Al, P, Ni, and O elements with a high content of Mg element. Compared with the results of Table 1, Mg, Al, and O elements come from the magnesium alloy substrate, Ni, P, Na and F elements come from electroless nickel process. Note that, in area I (the white area), the Mg content (44.71 wt%) is significantly lower than that in area II (the dark region) (80.16 wt%), while the Ni and P content is greater than that in the dark region. Thus, the Mg, Ni and P elements content in the white and the dark areas are quite different, which suggests that a discontinuous electroless Ni-P coating is deposited on the magnesium alloy substrate after electroless nickel for 1 min.

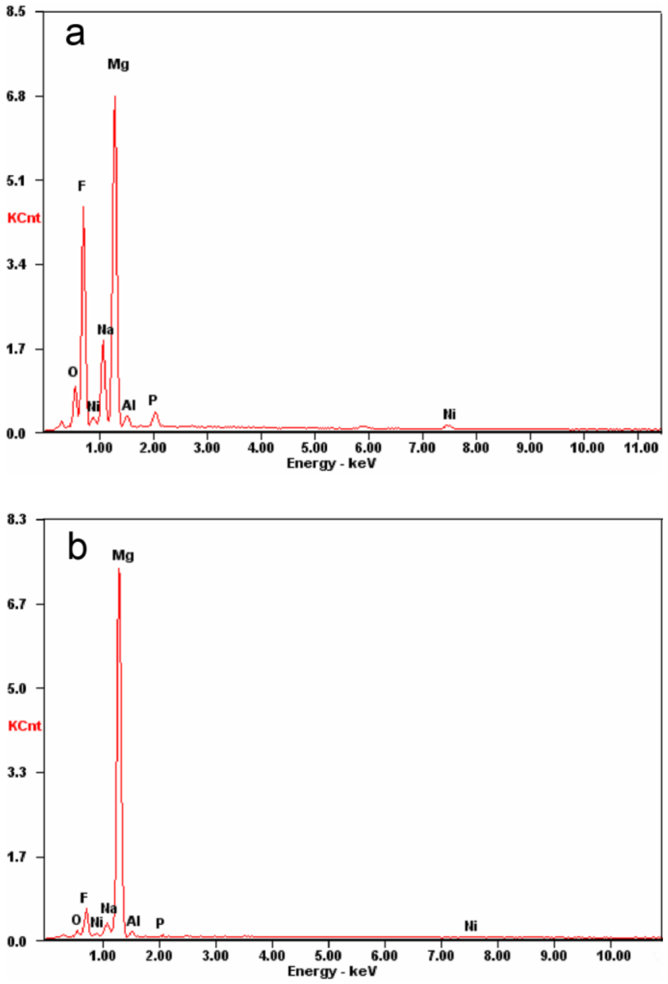

Figure 6. The corresponding EDS spectra of Ni-P coating showing in Figure 5, (a) area I(white region), (b) area II (dark region)

In addition, it also can be seen from Figure 6 and Table 2 that F element was detected in the initial EN deposits, and the F content is lower in the white area than in the dark area. It was reported by Rajan Ambat[17] that, when the magnesium alloy substrate is immersed into the F-containing electroless nickel bath, F^- will react with magnesium alloys to form MgF_2 film, and to improve the adhesion between the magnesium alloy and electroless Ni-P coating.

Table 2. Chemical compositions of magnesium alloy after electroless Ni-P for 1 min (in wt%) obtained by EDS analyses

Element	Wt%(area I)	Wt%(area II)
O	7.40	2.66
F	28.62	8.92
Na	11.88	3.39
Mg	44.71	80.16
Al	2.26	2.84
P	2.27	0.55
Ni	2.86	1.48

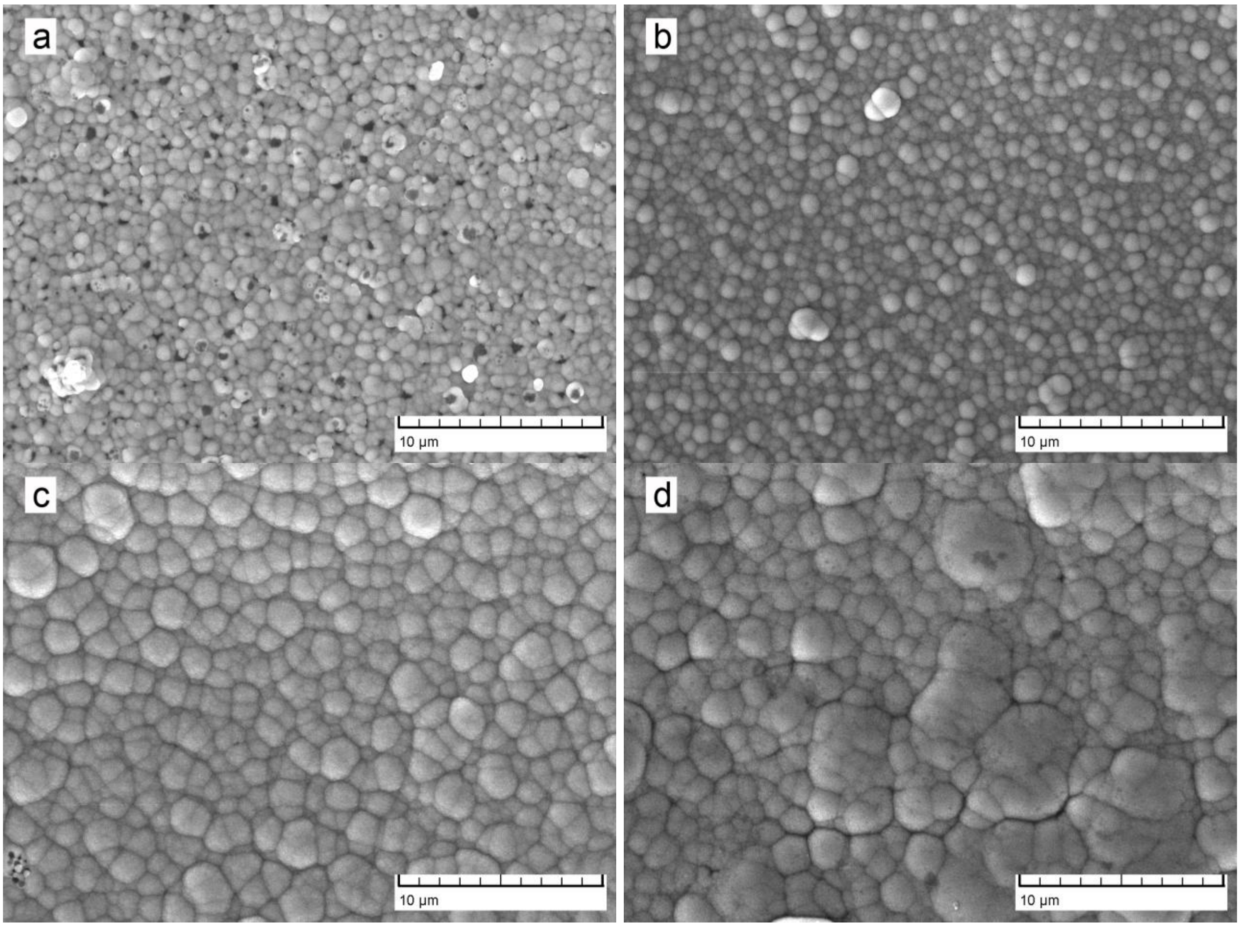

Figure 7. SEM micrographs of Ni-P coating deposited at different time, (a) 5 min, (b) 10 min, (c) 20 min, (d) 30 min

Figure 7 shows the SEM micrographs of Ni-P coating deposited at different time. According to Figure 7(a), a large number of small and compact Ni-P cells are uniformly distributed on magnesium substrate for depositing 5 min. However, there are many pores, indicating that Ni-P coating does not cover the magnesium alloy substrate surface completely. As the deposition time prolongs, the magnesium alloy substrate is fully covered by the electroless Ni-P coating and the Ni-P crystals grain grow up gradually. For example, the Ni-P coatings deposited for 20 min (Figure 7(c)) and 30 min(Figure 7(d)) were smooth and compact, shown as spherical nodular-like structure, which is in good agreement with other literature [12, 31].

In order to study the characteristics of electroless Ni-P deposition process, the open circuit potential-time curves of magnesium alloy samples in the electroless nickel bath at different temperatures was measured, and the results were shown in Figure 8.

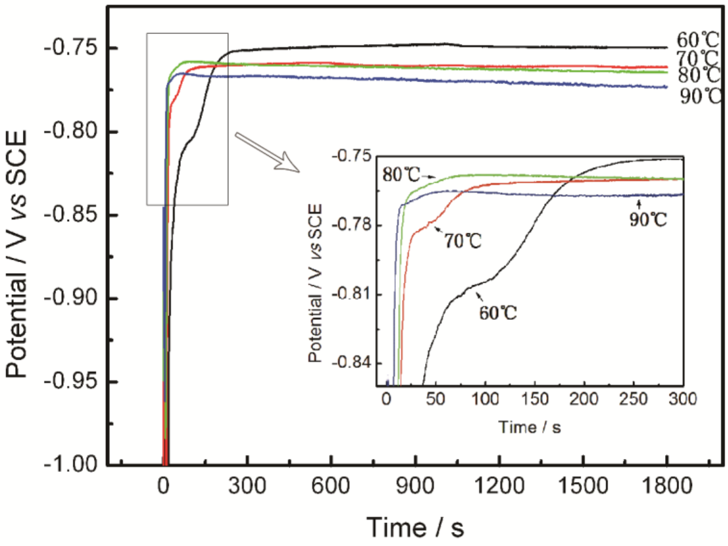

Figure 8. open potential-time curves of electroless Ni-P plating on magnesium alloy substrate in an electroless nickel bath shown in Table 1 at different temperature.

The open circuit potentials for all samples during electroless Ni-P plating process present obviously positive shift, and then stabilize. In these experiments, the positive shift time is within 300 s. The positive shift of open circuit potential should be related to the rapid formation of Ni-P coating on the magnesium alloy substrate. In addition, Figure 8 also shows that a higher temperature results in a shorter time to reach the stable potential, but the high temperature leads to a negative shifting of stable potential. This shows that a higher temperature will increase the deposition rate of electroless Ni-P plating.

It was reported by Rajan *et al*[17] and Zhenmin Liu *et al*[32] that the direct electroless nickel process on magnesium alloys included a initial galvanic coupling reaction (between the β phase and adjacent α phase) and electroless nickel deposition reaction on the β phase. However, as a highly active metal alloy and the heterogeneous microstructure of magnesium alloy, the direct electroless Ni-P plating on magnesium alloy is more complicated and the deposition process is still more difficult. As mentioned earlier in this paper (Figure 1- Figure 4), after phosphate pickling pretreatment, a discontinuous Mg-Mn phosphate film with some deep and wide cracks is formed on the surface of the magnesium alloy. Some of magnesium alloy substrate was possible to be exposed from the cracks in the film, forming magnesium oxide. The magnesium oxide will dissolve by dipping magnesium alloy into the electroless nickel solution, leaving the underlying magnesium alloy exposed to the bath. Thus, it's possible that there will be a displacement reaction between Ni and Mg substrate at the initial deposition stage, involving Mg atom dissolution, Ni^{2+} reduction and deposition on Mg substrate. Once the nickel nuclei are formed on the Mg substrate, the chemical deposition then occurs on the nickel nuclei. Based on the above analysis, the electroless Ni-P deposition process on Mg substrate could be represented as follows:

At the interface between the Mg substrate and the electroless nickel solution, at the partial anode (α phase), magnesium atom oxidizes and Mg substrate is dissolved:

$$Mg \rightarrow Mg^{2+} + 2e \qquad (6)$$

While at the partial cathode (β phase), Ni^{2+} reduces and deposits on the substrate:

$$Ni^{2+} + 2e \rightarrow Ni \qquad (7)$$

The chemical deposition then occurs on the nickel nuclei.

On the other hand, at the initial electroless nickel deposition stage, F ions in the electroless nickel plating solution will react with magnesium, which is confirmed by the experimental results that the Ni-P coating contain F element(Figure 6 and Table 2). This process could be deduced as the following:

$$2F^{-} + Mg \rightarrow MgF_2 \qquad (8)$$

3.3 Properties of electroless Ni-P coating

The properties of electroless Ni-P coating with phosphate pretreatment on magnesium alloy were investigated by monitoring the coating thickness, phosphorus content, hardness, and microstructure and corrosion resistance in this section. The thickness and the phosphorus content of Ni-P coating were analyzed by XRF. The coating thickness deposited for 60 min was 19.1 μm, while deposited for 30 min was only 12.8 μm. The phosphorous content of the Ni-P coating deposited on magnesium alloy for 60 min was 10.3 wt%, which is a high phosphorous coating.

The hardness of the Ni-P coating deposited at different time was obtained by micro-hardness machine. The Ni-P coating hardness deposited for 30 min was only about 372.5 HV, while deposited for 60 min was about 552.4 HV, indicating that the hardness values increase with increasing coating thickness. Moreover, the hardness of these Ni-P coatings is far higher than that of the Mg alloy substrate (about 93.2 HV). It is believed that the magnesium alloy coated by Ni-P coating would be expected to greatly improve the wear resistance.

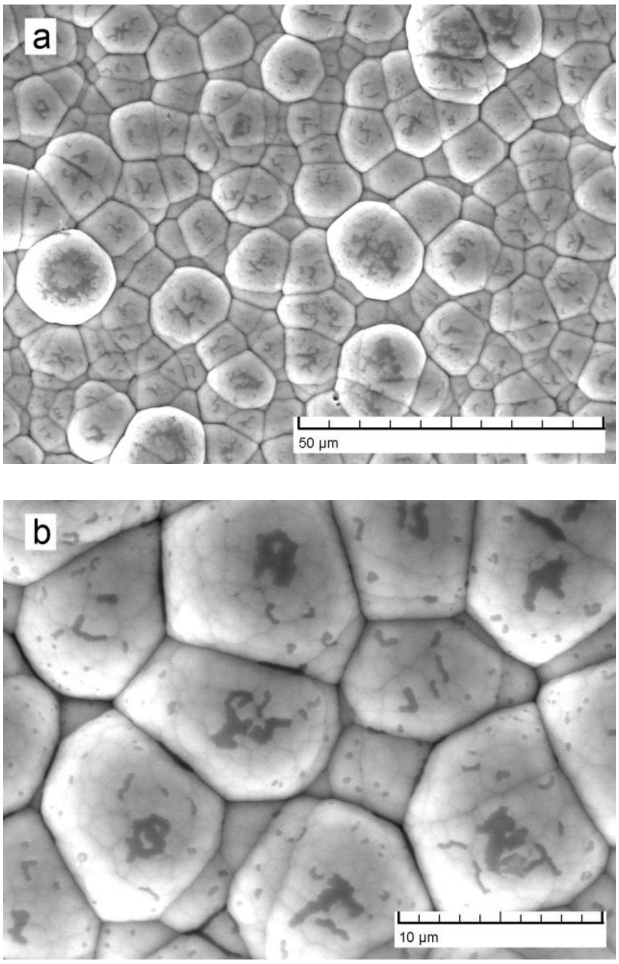

Figure 9. SEM micrographs, (a) electroless Ni-P coating on magnesium alloy deposited for 60 min; (b) a higher magnification of Figure 9(a).

The surface morphology of electroless Ni-P coating deposited on magnesium alloy for 60 min was shown in Figure 9. It can be seen that the Ni-P coating was compact, and uniformly covered the magnesium alloy surface, and there were no obvious defects such as pores or cracks on the coating surface. The Ni-P coating deposited for 60 min shows a spherical nodular-like structure, which is similar to that deposited for 30 min (Figure 7). Moreover, the Ni-P crystals cell size deposited for 60 min is much larger than that deposited only 30 min.

Figure 10 presents the cross-section microstructure and the corresponding EDS of electroless Ni-P coating after 60 min plating. The cross-section image Figure 10 (a) reveals that Ni-P coating was deposited on the Mg alloy substrate. There is no blistering, broken off or other evidence of poor adhesion in the cross-section area. The result shows that the adhesion between the Ni-P coating and the substrate is excellent. According to Figure 10(b), the chemical compositions of the area I was Mg, Al and Zn elements (Figure 10(a)); while the compositions of the area II were mainly determined to be Ni and P elements by EDS as Figure 10(c) showed.

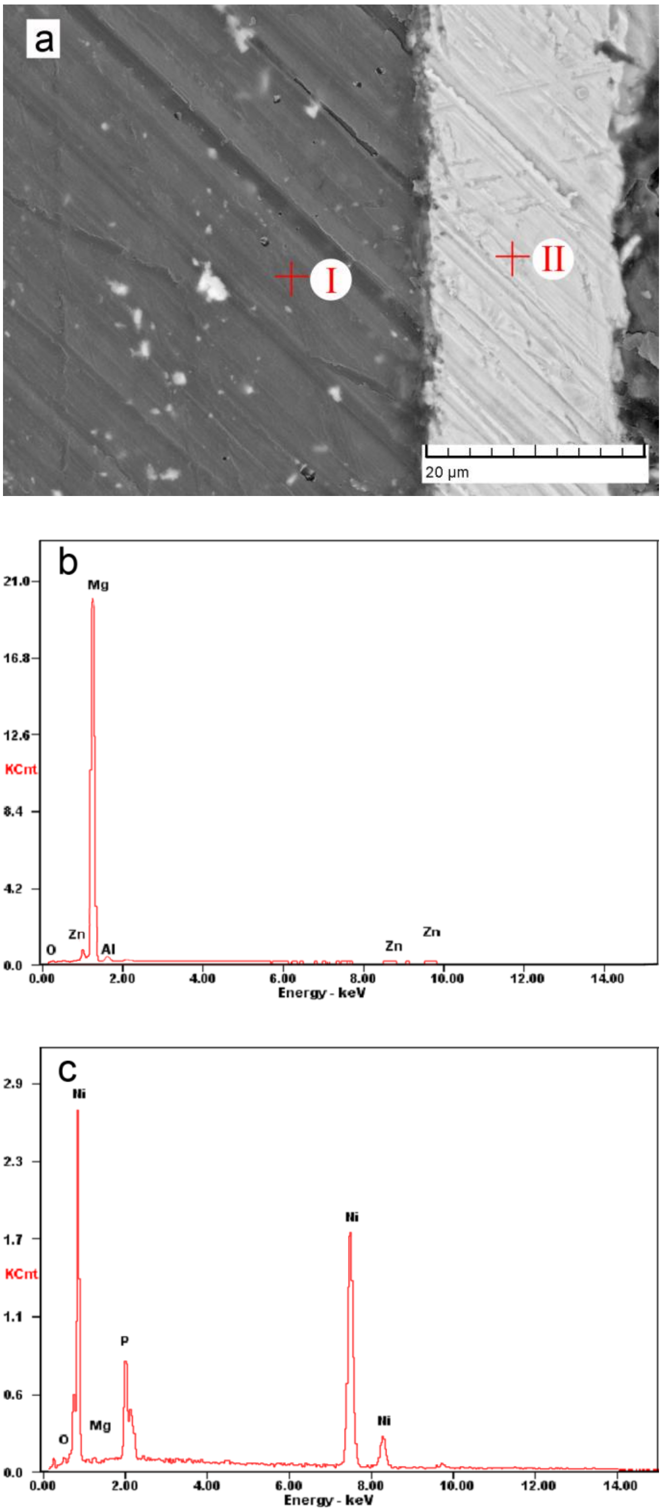

Figure 10. Cross-section microstructure and EDS spectra of Ni-P coating on magnesium alloy deposited for 60 min: (a) cross-section image; (b) EDS spectrum of area I; (c) EDS spectrum of area II.

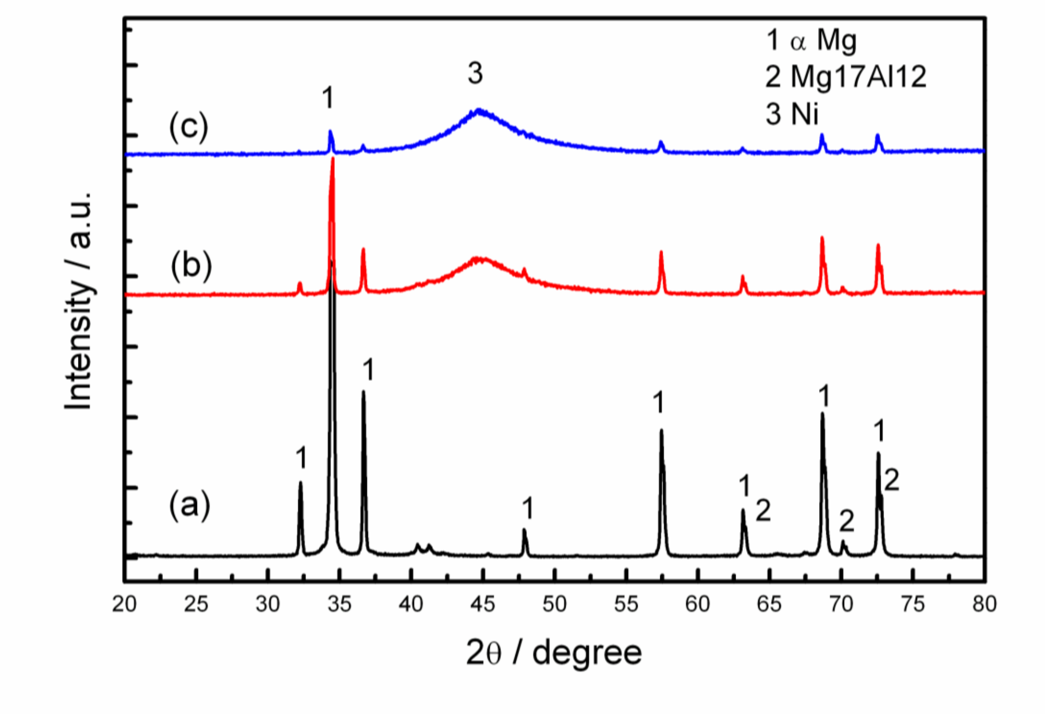

Figure 11. XRD patterns of AZ31 magnesium alloy in different surface states: (a) Mg alloy substrate; (b) electroless Ni-P coating for 30 min; (c) electroless Ni-P coating for 60 min.

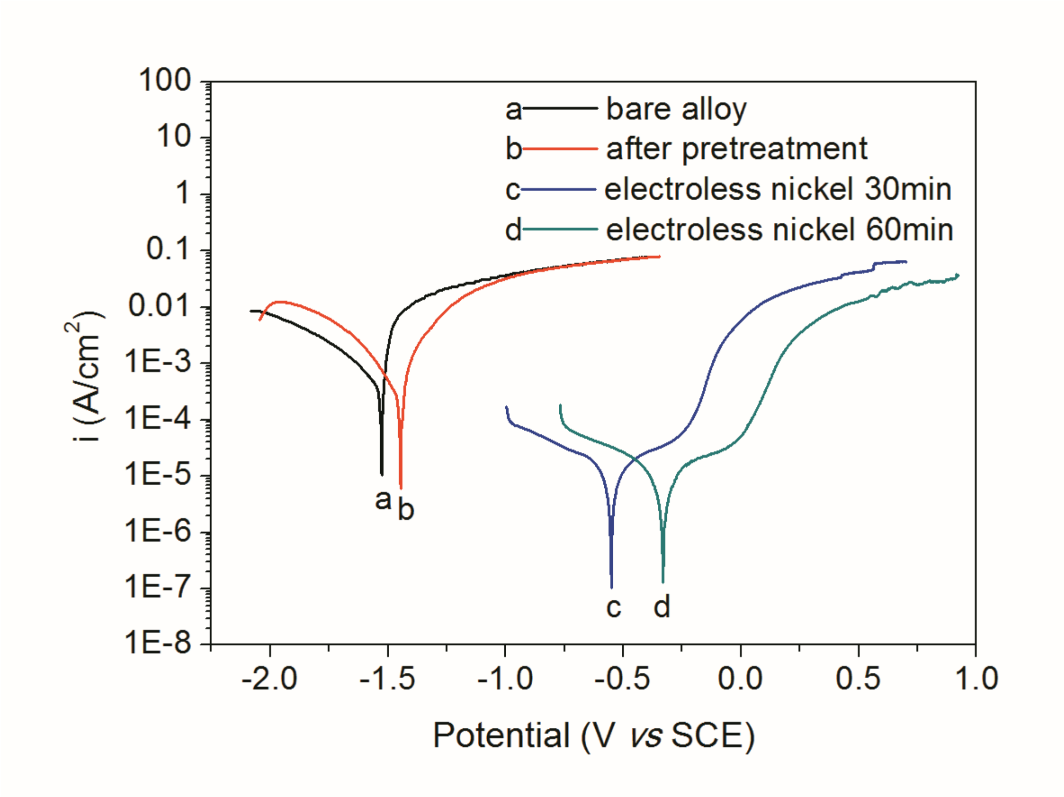

Figure 12. Potentiodynamic polarization curves of (a) bare magnesium alloy substrate, (b) after phosphate pickling pretreatment, (c) after electroless nickel 30 min and (d) after electroless nickel 60 min in 3.5wt% NaCl solution.

Fig. 11 displays the XRD patterns of the AZ31 magnesium alloy substrate at different surface states. The Mg alloy is mainly composed by Mg (α phase) and $Mg_{17}Al_{12}$ (β phase), which is given in Fig.11 (a). After electroless plating, the Mg alloy is fully covered by the as-plated electroless Ni-P coating, shown in the XRD pattern of Fig. 11 (b) and (c). It can be seen that a broad peak at 45° was located in these two electroless Ni-P coatings, which is considered to be related to the amorphous profile of Ni-P coatings[31, 33]. The result is consistent with the higher phosphorus content in the Ni-P coating.

The corrosion resistance of magnesium alloy with or without electroless Ni-P coating was investigated by potentiodynamic polarization methods in 3.5 wt.% NaCl solutions at room temperature, shown in Fig. 12. Noted that the main reaction in the cathodic branch of the polarization curves is hydrogen evolution, the anodic branch of the polarization curve can provide more information about the corrosion behaviors of magnesium alloy[16, 23]. For AZ31 magnesium alloy substrate (curve a) and the alloy treated by phosphate pickling (curve b), when the applied potential increased into the anodic branch, the polarization current increased with increasing the applied anodic potential and no passivation occurred, indicating that the anodic process was under activation control. The corrosion potential (E_{corr}) of magnesium alloy was -1.521 V *vs.* SCE, while the E_{corr} after treated by phosphate pickling was -1.439 V *vs.* SCE. The corrosion potential E_{corr} was shifted positively about 82 mV compared with that of magnesium alloy substrate and the corrosion current density i_{corr} decreased from 10.506 $\mu A/cm^2$ of the substrate to 6.279 $\mu A/cm^2$ of the sample treated by phosphate pickling.

The corrosion potential of electroless Ni-P coated for 30 min (curve c) and 60 min (curve d), were found to be -0.542 V *vs.* SCE and -0.323 V *vs.* SCE, and shifted by 979 mV and 1198 mV to the positivelt direction, respectively, as compared with that of magnesium alloy substrate (-1.521 V, curve a). And the corrosion current densities (i_{corr}) after electroless Ni-P coating were largely decreased than that of the substrate. Moreover, for the samples treated by electroless Ni-P coating, when the applied potential increased into the anodic region, an obvious passivity was observed. For both curve c and d, the passivation range reached 200 mV or so. Only when the applied anodic potential was high enough for passive film breakdown, the nickel dissolution would have occurred through the pores of Ni-P coating. Therefore, it can be deduced from the above discussion that the corrosion resistance and protection characterization of magnesium alloy substrate could be greatly improved by a pretreatment film and electroless Ni-P coating.

4. CONCLUSIONS

After phosphate pickling pretreatment, a Mg-Mn phosphate film was formed on AZ31 magnesium alloy surface, which makes the electrode potential of magnesium alloys shift to the positive direction.

An electroless Ni-P coating was directly deposited on the magnesium alloy after phosphate pickling pretreatment. During the electroless Ni-P plating process, the electrode potential shows obviously positive shift. The Ni-P coating was compact, and uniformly covered the magnesium alloy surface, with an amorphous profile, which is consistent with the higher phosphorus content. After electroless Ni-P plating for 60 min, the hardness of AZ31 magnesium alloy was 552.4 HV, which is far higher than that of the Mg alloy substrate (about 93.2 HV). The corrosion potential of electroless Ni-P coated for 60 min was found to be -0.323 V *vs.* SCE, and shifted by 1198 mV to the positive direction, as compared to magnesium alloy substrate. The corrosion resistance of the AZ31 magnesium alloy could be greatly increased by the formations of Mg-Mn phosphate film and electroless Ni-P coating

ACKNOWLEDGEMENTS

This work was financially supported by "the Fundamental Research Funds for the Central Universities" (Grant No. HIT. NSRIF. 2009155).

References

1. L. Wu, J. Zhao, Y. Xie, Z. Yang, T. *Nonferr. Metal. Soc*., 20 (2010) s630-s637.
2. Z. Liu, W. Gao, *Surf. Coat. Tech*., 200 (2006) 5087-5093.
3. X. Guo, M. An, P. Yang, H. Li, C. Su, *J. Alloys. Compd*, 482 (2009) 487-497.
4. G. Yan, W. Guixiang, D. Guojun, G. Fan, Z. Lili, Z. Milin, *J. Alloys. Compd*., 463 (2008) 458-461.
5. H.S. Ryu, S.H. Hong, *J. Electrochem. Soc*., 156 (2009) C298-C303.
6. Y.W. Song, D.Y. Shan, E.H. Han, *Electrochim. Acta*, 53 (2008) 2135-2143.
7. J.W. Tang, K. Azumi, *J. Electrochem. Soc.*, 158 (2011) D535-D540.
8. C. Gu, J. Lian, J. He, Z. Jiang, Q. Jiang, *Surf. Coat. Tech*., 200 (2006) 5413-5418.
9. H.S. Ryu, S.J. Mun, T.S. Lim, H.C. Kim, K.S. Shin, S.H. Hong, *J. Electrochem. Soc*., 158 (2011) C266-C273.
10. C. Zhong, F. Liu, Y. Wu, J. Le, L. Liu, M. He, J. Zhu, W. Hu, *J. Alloys. Compd*., 520 (2012) 11-21.
11. C. Zhong, M.F. He, L. Liu, Y.J. Chen, B. Shen, Y.T. Wu, Y.D. Deng, W.B. Hu, *Surf. Coat. Tech*., 205 (2010) 2412-2418.
12. W.X. Zhang, J.G. He, Z.H. Jiang, Q. Jiang, J.S. Lian, *Surf. Coat. Tech*., 201 (2007) 4594-4600.
13. M. AnIk, E. K Rpe, *Surf. Coat. Tech*., 201 (2007) 4702-4710.
14. N. El Mahallawy, A. Bakkar, M. Shoeib, H. Palkowski, V. Neubert, *Surf. Coat. Tech*., 202 (2008) 5151-5157.
15. Y. Zhu, G. Yu, B. Hu, X. Lei, H. Yi, J. Zhang, *Appl. Surf. Sci*., 256 (2010) 2988-2994.
16. H. Huo, Y. Li, F. Wang, *Corros. Sci*., 46 (2004) 1467-1477.
17. R. Ambat, W. Zhou, *Surf. Coat. Tech*., 179 (2004) 124-134.
18. X. Lei, G. Yu, X. Gao, L. Ye, J. Zhang, B. Hu, *Surf. Coat. Tech*., 205 (2011) 4058-4063.
19. L. Yang, J. Li, Y. Zheng, W. Jiang, M. Zhang, *J. Alloys. Compd*., 467 (2009) 562-566.
20. W.X. Zhang, N. Huang, J.G. He, Z.H. Jiang, Q. Jiang, J.S. Lian, *Appl. Surf. Sci*., 253 (2007) 5116-5121.
21. X. Cui, G. Jin, Q. Li, Y. Yang, Y. Li, F. Wang, *Mater. Chem. Phys*., 121 (2010) 308-313.
22. H.H. Elsentriecy, K. Azumi, *J. Electrochem. Soc*., 156 (2009) D70-D77.
23. J. Sudagar, J. Lian, X. Chen, P. Lang, Y. Liang, *T. Nonferr. Metal. Soc*., 21 (2011) 921-928.
24. W. Cheong, B.L. Luan, D.W. Shoesmith, *Corros. Sci*., 49 (2007) 1777-1798.
25. S. Zhang, Q. Li, X. Yang, X. Zhong, Y. Dai, F. Luo, *Mater. Charact*., 61 (2010) 269-276.
26. J. Li, Y. Tian, Z. Huang, X. Zhang, *Appl. Surf. Sci*., 252 (2006) 2839-2846.
27. J. Li, Z. Shao, X. Zhang, Y. Tian, *Surf. Coat. Tech*., 200 (2006) 3010-3015.
28. H. P. Liu, Y. Q. Wang, S. F. Bi and N. Li, *Electroplating & Pollution Control*, 30 (2010) 14-16 (in Chinese).

29. H. P. Liu, W. C. Xia, S. F. Bi and N. Li, *Electroplating & Finishing*, 30 (2011) 15-18 (in Chinese).
30. X. Liu, Z. Liu, P. Liu, Y. Xiang, W. Hu, W. Ding, *T. Nonferr. Metal. Soc*., 20 (2010) 2185-2191.
31. L. Zeng, S. Yang, W. Zhang, Y. Guo, C. Yan, *Electrochim. Acta*, 55 (2010) 3376-3383.
32. Z. Liu, W. Gao, *Surf. Coat. Tech*., 200 (2006) 3553-3560.
33. H. Liu, N. Li, S. Bi, D. Li, Z. Zou, *Thin Solid Films*, 516 (2008) 1883-1889.